International Journal of Applied Science and Engineering
2014. 12, 4: 257-274

A Control System Analysis of a Direct-Chill Cast Process of Aluminum Ingots by an Inverse Measured Method

Kun-Nan Lie*, Yen-Hsun Chen, and Meng-Tsun Tsai

Far East University Tainan, Taiwan, R.O.C.

Abstract: A direct-chill (DC) cast process of an aluminum ingot of size 3200×1292×320 mm^3 is analyzed numerically by the analysis of a fixed controlled system. The study investigates the DC processes in which liquid aluminum is cooling continuously in mold and then with water spray at the exit of mold. An inverse method is applied to measure heat transfer coefficient on water cooling surface experimentally. A correlation of heat transfer coefficient with surface temperature is used in numerical simulation. It has been approved that the defected curl and tears are caused by the higher rates of initial cooling and solidifying in mold and the sweat and liquation are caused by the isolation of heat transfer by air gap formed between cast solid surface and the mold wall by volume shrinkage with solidification. The present research analyzes the variations of temperature profiles in the cast ingot by the changes of cast speed and cast temperature and assesses the improvements of mold and cast process for the better cast quality.

Keywords: Aluminum casting; direct chill process; inverse method; liquid head.

1. Introduction

More than 90% aluminum is cast to be ingots or billets and then reformed to be required shapes of mechanical parts so that the cast quality decides the quality of manufactured aluminum parts. DC casting is widely used to produce aluminum ingots for the simplicity in its automated processes but it can induced cast defects by high cooling rates and non-equilibrium solidification conditions. The estimated 30-40% of aluminum should be wasted and recycled from the defected parts through casting and manufacturing processes and 10% is cut off from the cast ingot for the defects of curl, crack, sweat or liquation.

Since French Junghaus successfully developed vertical semi-continuous DC casting in 1933, the technique of DC casting has been widely researched for the applications of non-ferrous metals. Alcoa and Vlw companies successfully applied DC casting in the cast processes in 1935. Thereafter the continuous DC casting has been applied to the cast of aluminum alloys. Since Roth investigated the heat transfer in DC casting numerically in 1943, the numerical analysis has been an effective method to investigate the problems in DC cast processes and the correct results depend on the valid simulations of boundaries. The researches [1-3] on the cast defects of curl, crack and segregation found that the defects are related to the abrupt change of temperature profiles in the cast processes. And since then the temperature profiles in the DC casting have

* Corresponding author; e-mail: q6260@cc.feu.edu.tw

© 2014 Chaoyang University of Technology, ISSN 1727-2394

Received 25 July 2013
Revised 24 June 2014
Accepted 8 July 2014

been the interest of researchers. Weckman [4] employed a two dimensional steady-state model by use of finite-element analysis to investigate the correlations of heat transfer to surface temperature in a semi-continuous casting of a cylindrical aluminum ingot. Mortensen [5] analyzed the heat transfer in the initial stage of casting of flat slabs by a three-dimensional model during the phase change from liquid to solid in which the thermal properties are functions of temperature. Drezet [6-7] formulated the transient governing equations and fixed the coordinates on the cast ingot to analyze the temperature variations. Prasso [8] formulated the steady-state governing equations by the assumption of steady cast speeds and the method of a fixed control volume to analyze the temperature variations in the cast ingot. Xie [9] analyzed the cast process of cylindrical aluminum cast ingots numerically by use of three-dimensional finite-element and designed an experiment to correlate the heat transfer coefficients to the surface temperatures of an aluminum ingot. Dua *et al.* [10] investigated the effects of ramping casting speeds and temperatures on the temperature distributions and melted flow patterns in the sump of a DC cast billet of aluminum alloy. Lalpoor *et al.* [11] investigated cold cracking in DC cast of high strength aluminum alloy ingots by numerical simulations to predict the critical crack size distributions at various casting conditions for cold cracking to occur.

The present paper investigates the DC casting process of an aluminum ingot of size $3200\times1292\times320$ mm^3 and analyzes the variation of temperature in cooling process by numerical analysis. A method of fixed control volume of total mass of the aluminum ingot and a correlation of heat transfer coefficient by Xie [9] are adopted. The purpose is to investigate the effects of casting speed and temperature on the solidification in which the head of liquid in cast ingot is considered to induces the cast defects relatively.

2. Analysis method

The schematic illustrations of DC casting are shown in Figure 1. The liquid aluminum is poured into the cavity of mold from the top and then the bottom block of mold starts to move down the solidified ingot until the assigned length is reached and the solid cast is removed to standby for next procedure. The length of ingot can't be extended unlimited and the DC casting is called to be semi-continuous casting process. The primary cooling takes place in mold by the wall heat conduction in which the solid shell is formed and then the air gap between the cast and mold wall is formed by shrinkage in solidification. The air gap makes the heat conduction fall down. The secondary cooling takes place at the exit of mold by the cold water spray against the cast wall that increases the heat transfer from the cast again.

A fixed control system of total cast mass is taken for the numerical simulation for the cooling processes as shown in Figure 2. The total mass of aluminum is of the same melted temperature initially. The mold and water spray are simulated to rise from the bottom of mold in cast speed in the cooling process. This model of a fixed system makes sure of conservation of total energy. The heat transfer takes place only between the cast aluminum and mold and water spray.

During the casting, the governing equation of heat transfer is written as:

$$\frac{\partial}{\partial x}\left(k\frac{\partial T}{\partial x}\right)+\frac{\partial}{\partial y}\left(k\frac{\partial T}{\partial y}\right)+\frac{\partial}{\partial z}\left(k\frac{\partial T}{\partial z}\right)+Q_v=\rho c_p\frac{\partial T}{\partial t} \tag{1}$$

Where T is temperature, x y z are the Cartesian coordinates, t is time, k is the conductivity of aluminum, Qv is the heat source of unit volume, ρ is the density of aluminum and cp is the specific heat capacity of aluminum. The thermal properties of aluminum are functions of

temperature as listed in Table 1. The heat source Qv in equation (1) represents the latent heat released by solidification. For simplicity, an equivalent specific heat capacity $C_{Pe}= C_P+ \frac{L}{T_L-T_S}$ is employed to eliminate Qv in equation (1) and equation (1) is simplified as:

$$\frac{\partial}{\partial x}\left(k\frac{\partial T}{\partial x}\right)+\frac{\partial}{\partial y}\left(k\frac{\partial T}{\partial y}\right)+\frac{\partial}{\partial z}\left(k\frac{\partial T}{\partial z}\right)=\rho C_{pe}\frac{\partial T}{\partial t} \tag{2}$$

where L is the latent heat, T_L is the initial liquid temperature and T_S is solidification temperature.

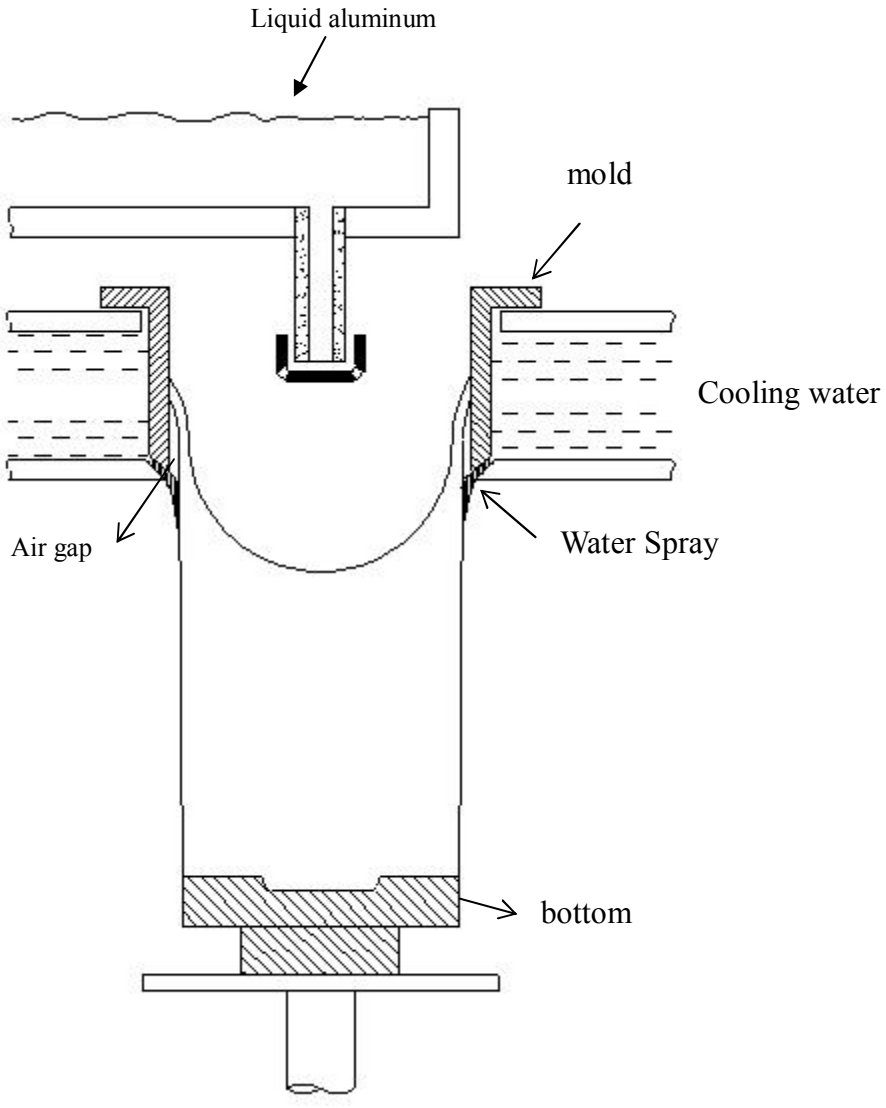

Figure 1. The schematic illustrations of DC casting

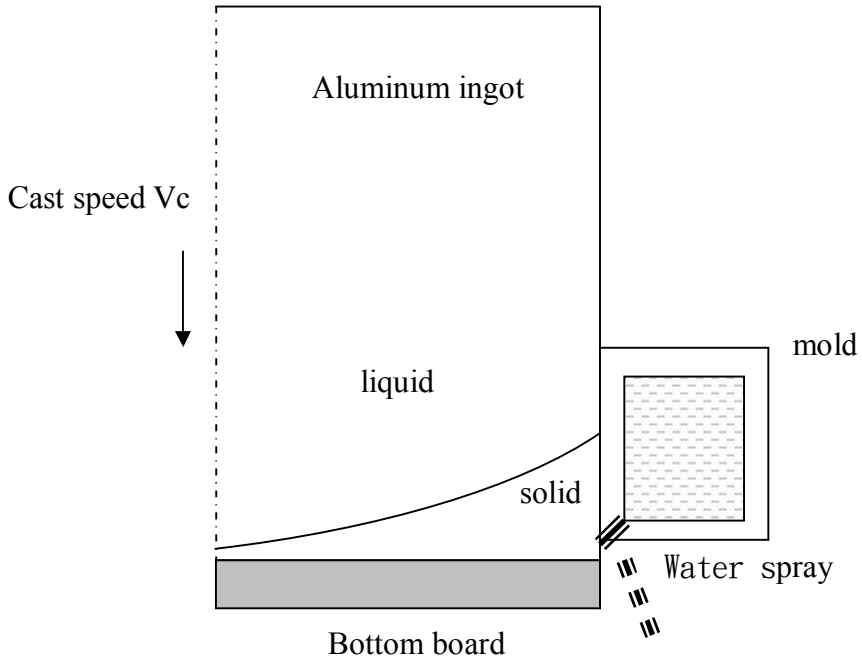

Figure 2. Numerical simulation of fixed total cast mass

Table 1. The thermal properties of aluminum as functions of temperature

Temperature (℃)	100	200	400	660	800
Specific heat capacity C_p J/(Kg × °K)	482	798	949	1127	1146
Conductivity k W/(m ×°K)	302	237	240	97	97
Density ρ (kg/m^3)	Solid ρ=2699			Liquid ρ=2365	

For the boundary condition of cooling in mold, The heat transfer coefficient h of 2000 W/(m^2·°K) is adopted for liquid aluminum as asserted by Adrian Sabau *et al.* [12] and the reduced heat transfer coefficient h of 200 W/(m^2·°K) is adopted for solidified aluminum for the air gap isolation. At the exit of mold, water spray impinges on the cast surface and causes intensive cooling in which the heat transfer coefficienth depends on the mode of boiling and is a function of surface temperature. We take advantage of Xie [11] in which the values of heat transfer coefficient h are determined reversely by an experiment to measure the heat flux on the cast surface under water spray as:

$$q_x = -k\frac{\partial T}{\partial x} \tag{3}$$

The convection equation is written as:

$$q_x = h(T_W - T_A) \tag{4}$$

Equating equations (3) and (4),

$$h = \frac{-k\partial T}{(T_W - T_A)\partial x} = \frac{-k\Delta T}{(T_W - T_A)\Delta x} \tag{5}$$

the values of heat transfer coefficient h can be calculated by measuring the temperature distribution in the experiments by Xie [11] as shown in Figure 3. The values of heat transfer coefficient h is a function of surface temperature and increases steeply as the surface temperature decreases from 400°C to 130°C and reach about the maximum 23000 W/(m^2·°K) and then decreases rapidly for further cooling down from 130 °C.

3. Numerical analysis

A finite difference scheme is employed to simulate the governing equation (2) and compute the temperature distribution in cast aluminum ingot numerically. The differential grids are planned as shown in Figure 4. The mold rises from the bottom in cast speed reversely to simulate the descent of the aluminum ingot in cooling process. The water spray follows the mold at the exit of mold for the secondary cooling. The cooling is symmetric to x and y axes and so as the temperature distribution. A quarter of total ingot is computed for the grid points and a grid size of 25×25×500 in x, z and y directions is enough to obtain a convergent result. The central difference is applied to the x, y and z coordinates. The forward difference is applied to the time step. The difference equation of the governing equation (2) is written as:

$$\frac{1}{\alpha}\left(\frac{T^{P+1}-T^{P}}{\Delta\tau}\right) = \frac{T_{i+1}+T_{i-1}-2T_i}{(\Delta x)^2} + \frac{T_{j+1}+T_{j-1}-2T_j}{(\Delta z)^2} + \frac{T_{k+1}+T_{k-1}-2T_k}{(\Delta y)^2} \tag{6}$$

$$\alpha = \frac{k}{\rho C_{Pe}} \tag{7}$$

During the cooling process, the thermal properties of aluminum ingot is functions of temperature and the thermal resistance algorism is employed to reformulate equation (6) as:

$$\sum_j \frac{T_j^P - T_i^P}{R_{ij}} = C_i \frac{T_i^{P+1} - T_i^P}{\Delta\tau} \tag{8}$$

for computing renewed temperature T_i^{P+1} after a time step. It is noted that the convergent solutions are obtained with a required criterion of the time step as:

$$\Delta\tau \le \left[\frac{C_i}{\sum_j \frac{1}{R_{ij}}}\right] \tag{9}$$

4. Results and discussions

The present paper simulates the DC casting processes numerically and investigates the heat transfer to analyze the cast defects in aluminum ingots and assess the availability of improvements. The material and process parameters are shown in Table 2. The frequent defects in cast processes are shown in Figures 5~10. Figure 5 shows the breed-out which occurs in the bottom of ingot and is caused by reheating for the air gap between the solidified ingot and mold isolates the cooling. Figure 5 also shows the curl in the bottom that result from the quick shrinkage by sudden cooling. The method of improving the curl is to reform the flat bottom mold to be convex to compensate the curl as shown in Figures 6 and 7. Figure 8 shows the cold shut on the bottom sides. The cold shut forms by the faster cooling speed in the starting stage of

casting. It can be conceived that the abrupt cooling in the beginning of casting give rise to the defected surface quality. Figure 9 shows the liquation inside of ingot. The liquation is located above the bottom ingot as air gap isolates the cooling and the solid cast is melted through by liquid cast. The liquation location becomes longer as the liquid head increases. Figure 10 shows the laps which has the pitch of about the span of three fingers. The laps form for the poor flood in the corner of mold.

The present numerical simulation of the casting process can help observe the temperature profile and the solidification and then analyzing the cast defects. Figures 11-16 show the isothermals in the central symmetric plane of ingot in different stages. Figure 11 shows the isothermals of cast as the cast descends 6.41 mm from mold and also as 6 seconds from the start of casting. It can be seen that the isothermals align over the bottom board and adjacent to side wall of mold at the start of casting and that the strong heat transfer and quick solidification take place over the contact surfaces. The quick solidification can be followed with the curl by the shrinkage of cast. Figure 12 shows the isothermals of cast as the cast descends 160 mm from mold and also as 141 seconds from the start of casting. It can be seen that area A is inside of mold and area B is outside of mold. The area A is the primary cooling with heat conduction to the mold wall and the area B is the secondary cooling with the water spray impinging upon the cast surface. The thickness and density of isothermals grow slowly as the cast exits from the mold for the water spray enhances cooling on the solidified surface. Figure 13 shows the isothermals of cast as the cast descends 321 mm from mold and also as 283 seconds from the start of casting. The isothermals in mold of area A grow slowly as compared with secondary cooling of area B that is the effect of heat isolation of the air gap inside of the mold. Figure 14 shows the isothermals of cast as the cast descends 641 mm from mold and also as 565 seconds from the start of casting. The isothermals of areas A and B reach to a steady condition. Figure 15 shows the isothermals of cast as the cast descends 1600 mm from mold and also as 1411 seconds from the start of casting. The isothermals are same as a steady condition. It is observed that the defects of cast as shown in Figures 5-10 are located in the bottom areas in which the isothermals are not developed steadily as shown in Figures 11 and 12. The defects are rarely found in the upper areas in which the isothermals are developed steadily as shown in Figures 13-15. Figure 16 shows the isothermals of cast as the cast descends 3200 mm from mold and also as 2820 seconds from the start of casting when the cast leaves the mold. The isothermals spread vertically as parallel to the cast surface. The heat transfer flows to surface which is cooled by water spray and the solid shell develops parallel and evenly to the center area of cast. The cast continue cooling in the air after it leaves the mold. A hook is dipped into the liquid top surface and ready for transportation when the top surface is cooled and solidified.

Figure 17 shows liquid head of cast as the cast descends 321 mm from mold and also as 283 seconds from the start of casting. The area A of isothermal represents the solid shell in which the temperatures are lower than solidifying temperature 660 ^{o}C. It can be measured that the depth of liquid head is 65×6.41=416 mm. The substantial liquid head results from the large mass of aluminum and fast cast speed of 68 mm/min. Figure 18 shows liquid head of cast as the cast descends 641 mm from mold and also as 565 seconds from the start of casting. It can be seen that the thickness of solid shell increases as the casting proceeds but that the depth of liquid head also increases to be (115-35)*6.41=513 mm and grows 97 mm. It is found that the solid shell and liquid head grows after the start of casting. Figure 19 shows liquid head of cast as the cast descends 1600 mm from mold and also as 1411 seconds from the start of casting. It is half way of cast process at this stage. The solid shell grows slowly to the center area. But the liquid head decreases to be (265-189)*6.41=487 mm and reduces 26 mm. The increased mass of bottom area

helps cooling of liquid cast. Figure 20 shows liquid head of cast as the cast descends 3200 mm from mold and also as 2820 seconds from the start of casting. The cast leaves the mold completely and the water spray finishes the cooling at this stage. It can be seen that the solid shell grows thicker and more even up to the top surface. The liquid head decreases more to be (500-438)*6.41=397 mm and reduces 116 mm. The cast stands by and continues with air cooling until solidifying completely. Figure 21 shows the temperature transitions during casting on the vertical edge of x-y planes. The lines A, B, C, D, E, F, and G are the temperatures of points of height 0, 160, 320, 480, 640, 960 and 1280 mm on the vertical edge of x-y planes. The horizontal line H represents solidifying temperature 660 ^{o}C. It can be seen that line A has no buffer time to solidify as crossing solidifying temperature 660 ^{o}C by the sudden cooling of bottom plate of mold. The sudden cooling causes the defected surface of curl, sweat and cold shut on the bottom of cast. Figure 22 shows the temperature cooling rates during casting on the vertical edge of x-y planes. Each line has two peaks that represent the cooling inside and outside of mold respectively. The front peak F1 is the cooling rate inside of mold that the air gap inside mold makes the fall down of cooling rate. The back peak F2 is the cooling rate by water spray outside of mold that the water spray makes a greater rise and fall of cooling rate by the boiling heat transfer. It can also be seen that the front peak of line A is higher than others for the bottom board of mold absorbs extra heat from the cast.

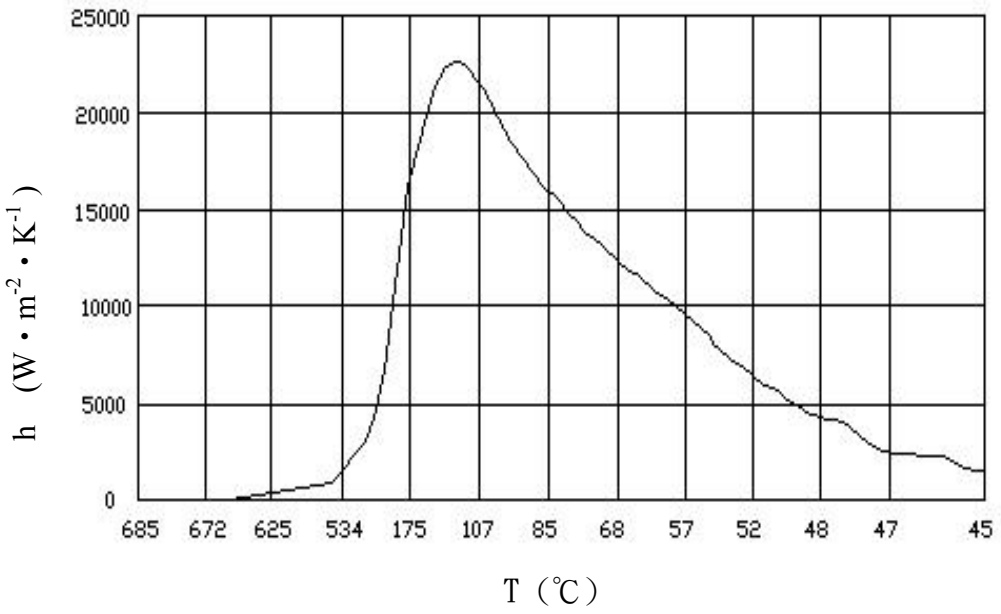

Figure 3. Heat transfer coefficient h vs. measured surface temperature T by Xie [11]

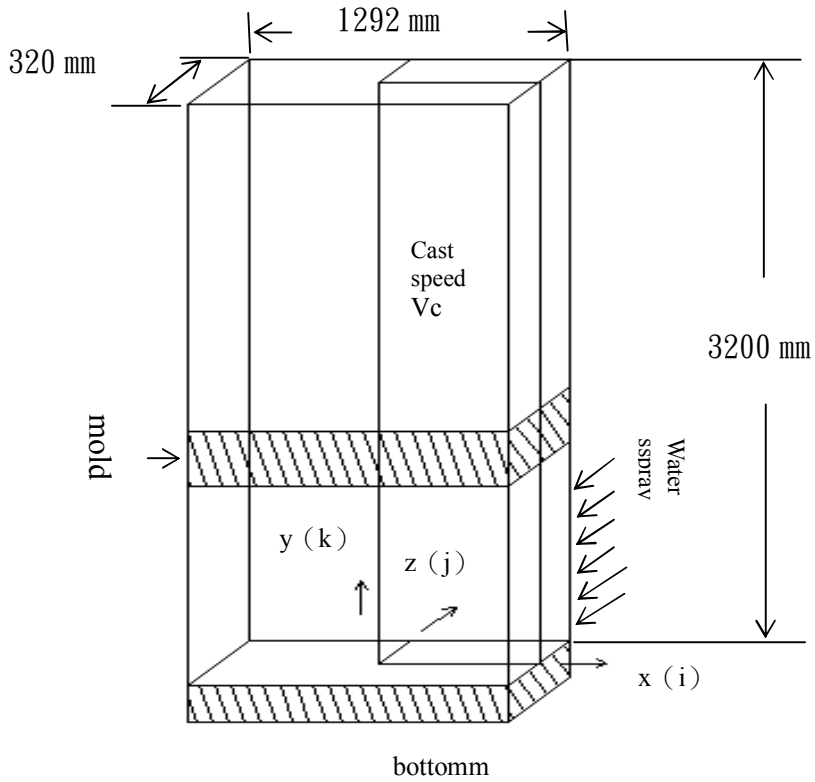

Figure 4. The schematic three dimensional numerical physical model

Figure 5. The breed-out in the bottom of ingot

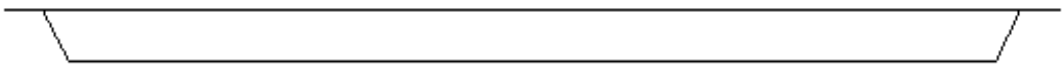

Figure 6. Flat bottom mold

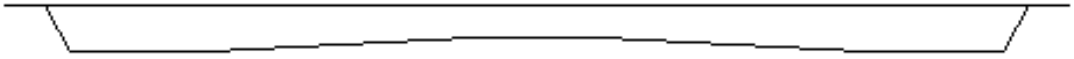

Figure 7. Convex bottom mold

Figure 8. Cold shut on the bottom sides

Figure 9. Liquation inside of ingot

Figure 10. Laps which has the pitch of span of three fingers

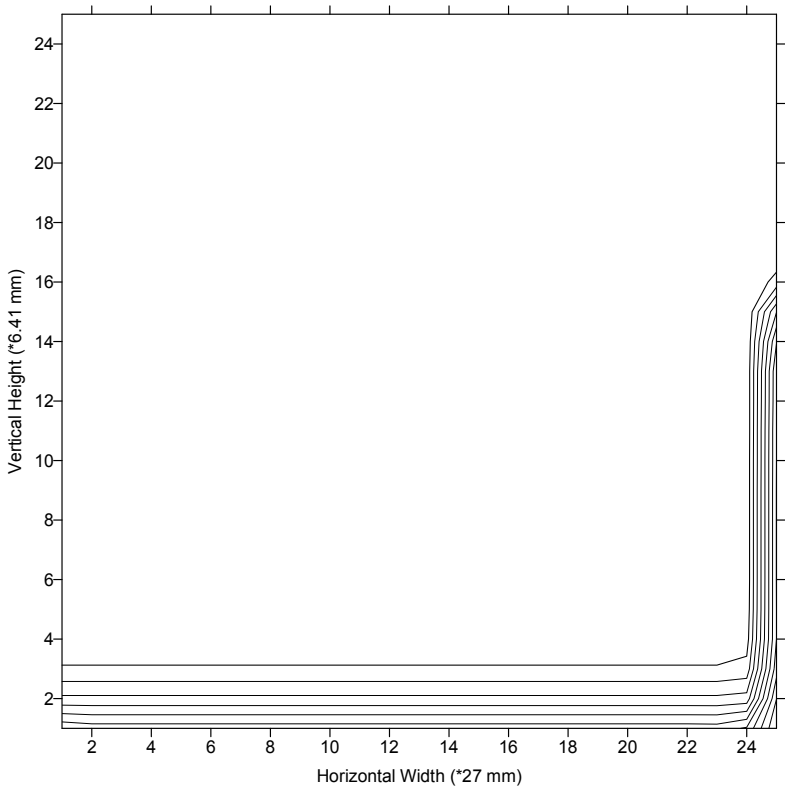

Figure 11. Isothermals of symmetric plane of cast as the cast descends 6.41 mm from mold and also as 6 seconds from the start of casting

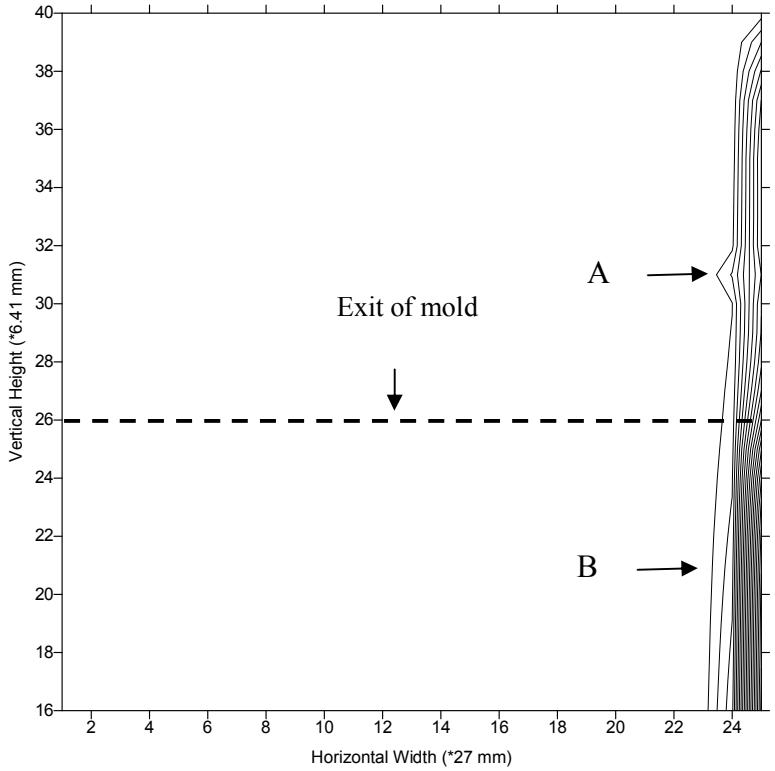

Figure 12. Isothermals of symmetric plane of cast as the cast descends 160 mm from mold and also as 141 seconds from the start of casting

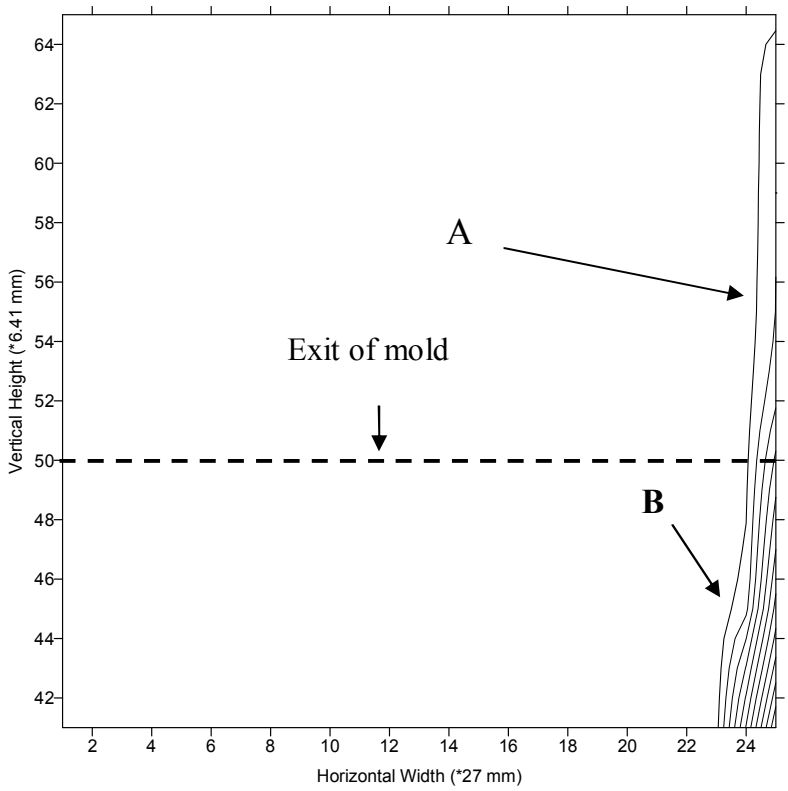

Figure 13. Isothermals of symmetric plane of cast as the cast descends 321 mm from mold and also as 283 seconds from the start of casting

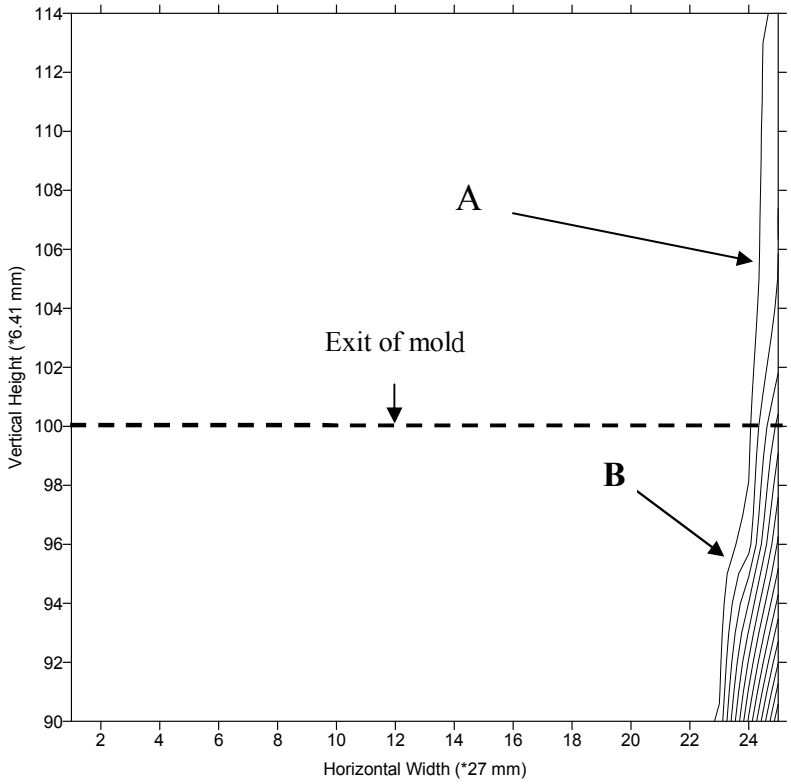

Figure 14. Isothermals of symmetric plane of cast as the cast descends 641 mm from mold and also as 565 seconds from the start of casting

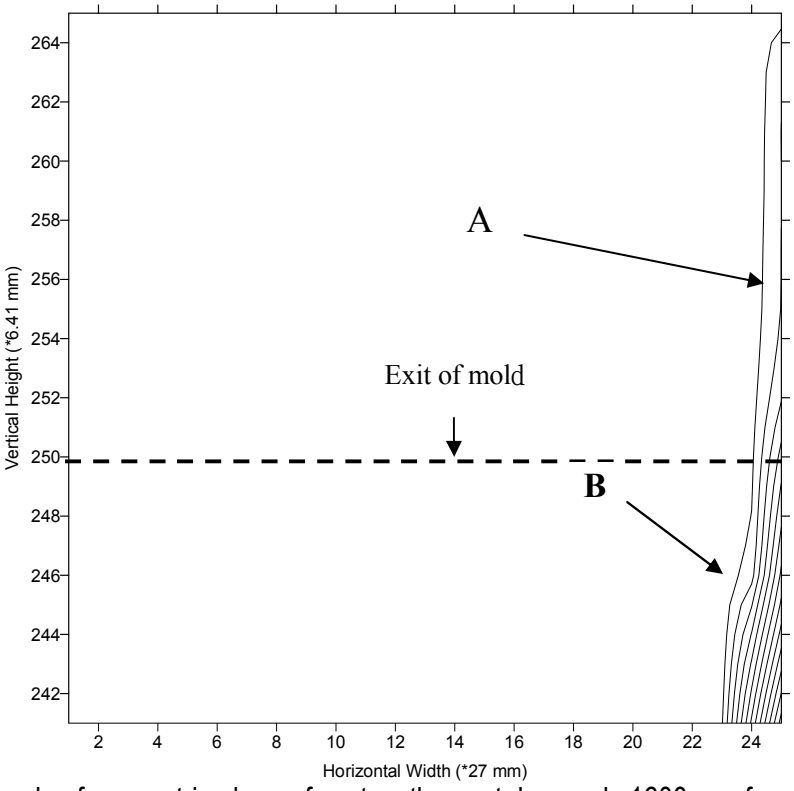

Figure 15. Isothermals of symmetric plane of cast as the cast descends 1600 mm from mold and also as 1411 seconds from the start of casting

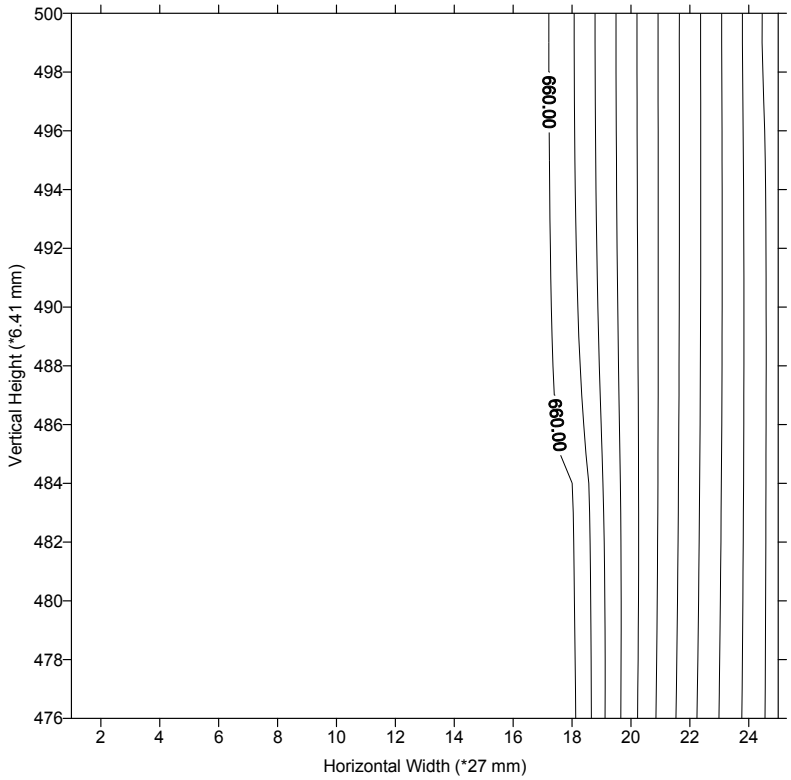

Figure 16. Isothermals of symmetric plane of cast as the cast descends 3200 mm from mold and also as 2820 seconds from the start of casting (finished of casting)

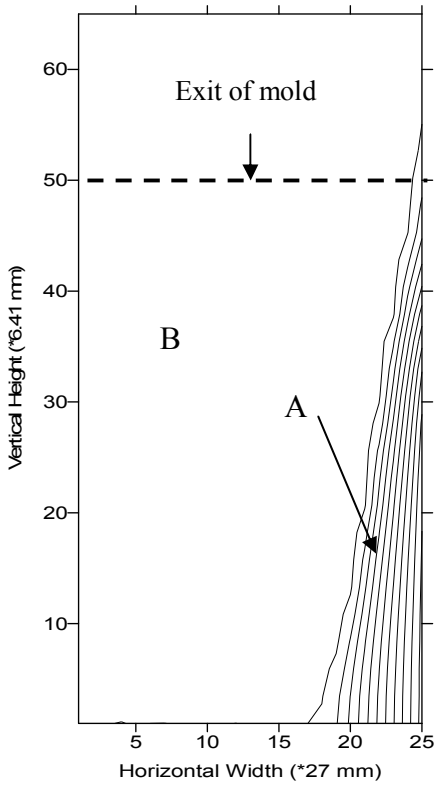

Figure 17. Liquid head of cast as the cast descends 321 mm from mold and also as 283 seconds from the start of casting

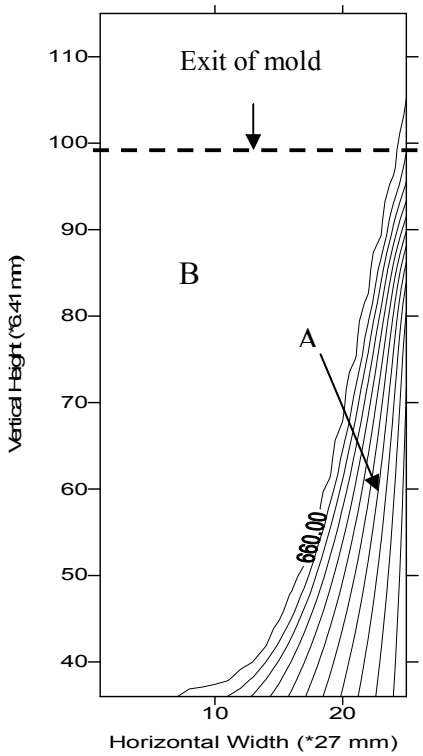

Figure 18. Liquid head of cast as the cast descends 641 mm from mold and also as 565 seconds from the start of casting

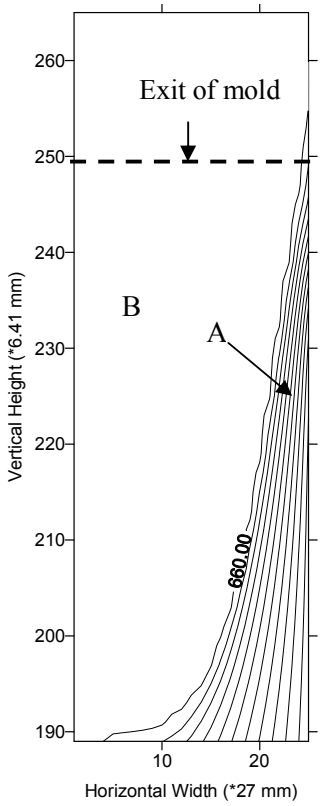

Figure 19. Liquid head of cast as the cast descends 1600 mm from mold and also as 1411 seconds from the start of casting

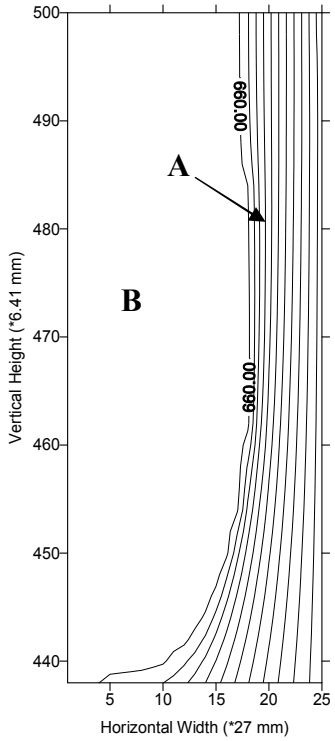

Figure 20. Liquid head of cast as the cast descends 3200 mm from mold and also as 2820 seconds from the start of casting (finished of casting)

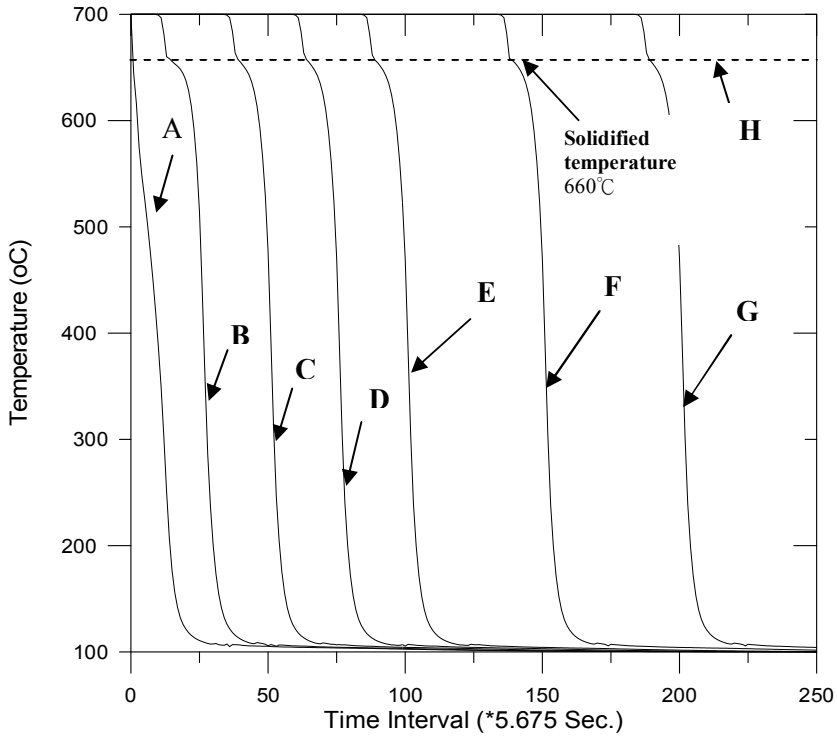

Figure 21. Temperature transitions on the vertical edge of x-y planes (A, B, C, D, E, F, and G are points of height 0, 160, 320, 480, 640, 960 and 1280 mm)

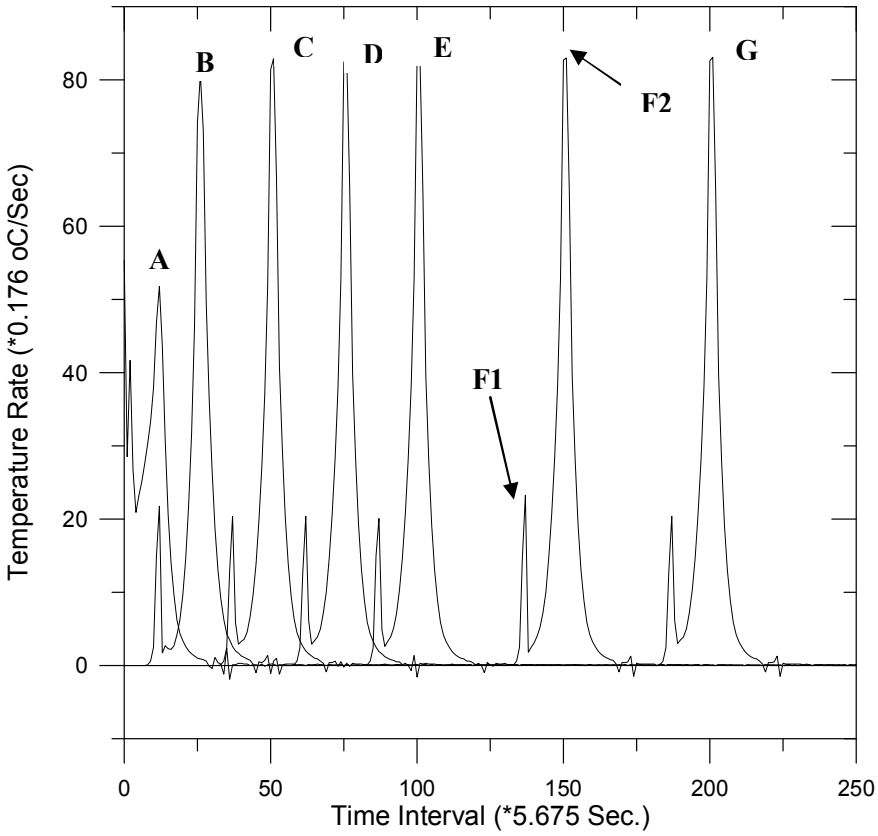

Figure 22. Temperature cooling rates on the vertical edge of x-y planes (A, B, C, D, E, F, and G are points of height 0, 160, 320, 480, 640, 960 and 1280 mm)

Figure 23 shows the liquid head for different cast speeds V_c = 0.00113 and 0.000565 (m/s) respectively. It is seen that the liquid head reduces over a half when the cast speed reduces to half of V_c = 0.00113 (m/s). It is apparent that at faster cast speed the liquid head increases and then decreases in cast process but that at slower cast speed the liquid head decreases consecutively in cast process. The faster cast speed makes the higher liquid head and causes defected cast quality so that the slower cast speed can improve cast quality. Figure 24 shows the liquid head for different cast temperatures T = 680 and 700 ^{o}C respectively. It is seen that there is no significant difference in liquid head. The effect of cast temperature can be neglected by little difference in liquid head. Figure 25 and 26 shows liquid head of cast as the cast descends 321 mm from mold for cast speeds at 0.00113 and 0.000565 (m/s) respectively. The comparison shows that at the reduced half cast speed the liquid head decreases and the thickness of solidified shell increases and therefore the casting has the better cast quality at the lower cast speed.

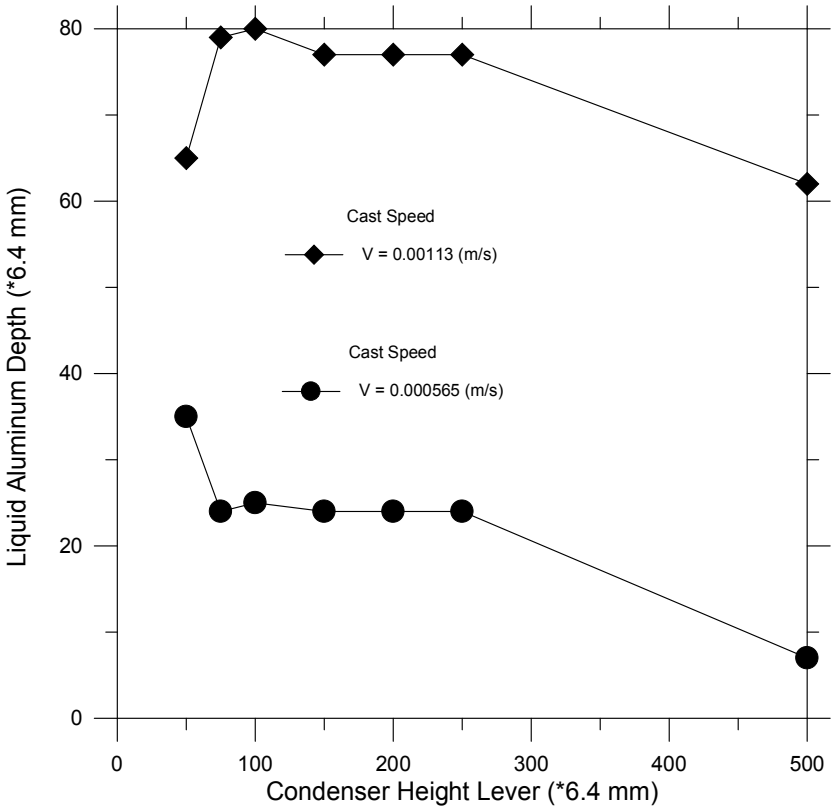

Figure 23. Liquid head for different cast speeds V_c = 0.00113 and 0.000565 (m/s) respectively

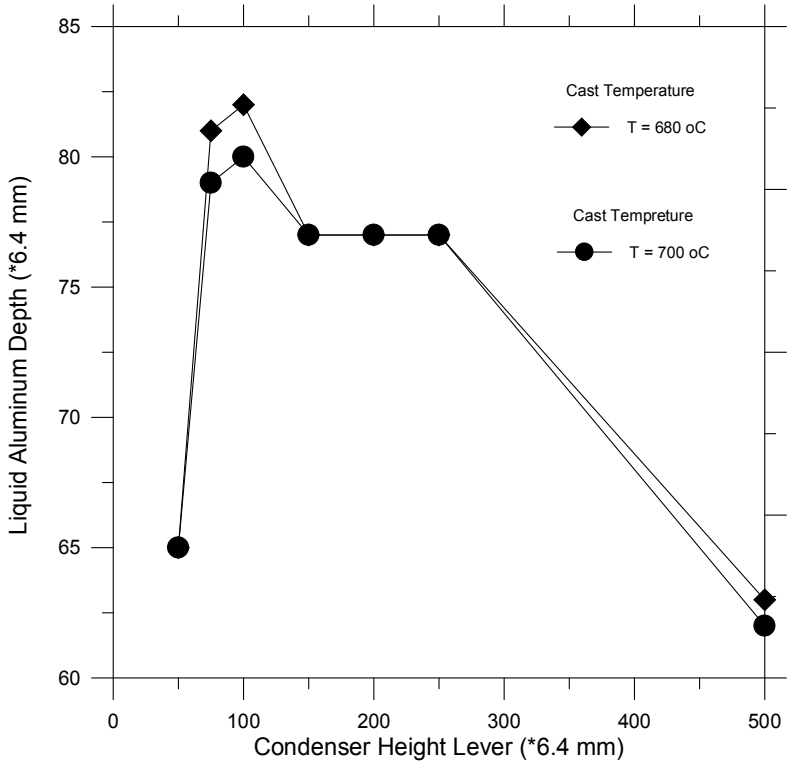

Figure 24. Liquid head for different cast temperatures T = 680 and 700 ^{o}C respectively

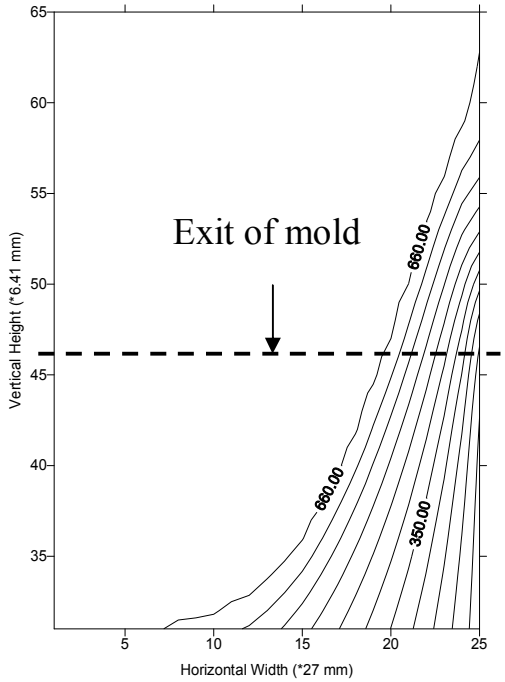

Figure 25. Liquid head of cast as the cast descends 321mm from mold for cast speeds at 0.000565 (m/s)

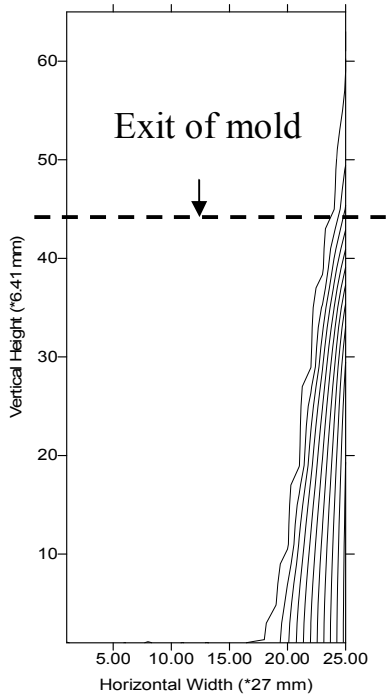

Figure 26. Liquid head of cast as the cast descends 321 mm from mold for cast speeds at 0.00113 (m/s)

5. Conclusions

The numerical analysis is employed to simulate DC casting in real manufacturing process. The temperature profile, liquid head and solidified shell are calculated to investigate the defects of the aluminum ingot. The following are concluded for improving the cast quality:

(1) The most defects appear in the bottom area of an aluminum ingot including curl, bleed out

and cold shut that are caused by a high cooling rate by mold bottom. In order to avoid the cooling rate, the mass of mold bottom gas to be reduced.

(2) The convex mold bottom can compensate the curl in the bottom of aluminum ingot that are caused by volume shrinkage in solidified aluminum.

(3) The casting of massive aluminum ingot can have high liquid head which causes the defects of reheat and bleed out. The slower cast speed can reduce the liquid head effectively and improve the defects.

(4) The cast temperature is not a significant factor affecting liquid head and cast quality.

(5) The slower cast speed can improve the cast quality but increases the cycle time of process and the manufacturing cost. It is a compromise between the cast quality and cost for determining an adequate cast speed.

References

[1] Drezet, J. M., Rappaz, M. et al. 2000. Determination of Thermophysical Properties and Boundary Conditions of Ddirect-Chill Cast Aluminum Alloys Using Inverse Methods. *J. Metal Mater Tran.*, 31B.: 1627-1634.

[2] Grandfield, J. F., Hoadley, A. and Instone, S. 1997. Synthesis and photophysical properties of a new cationic water-soluble Zn phthalocyanine. *J. Light Metals*, 691-699.

[3] Maner, L., Magnin, B. and Caratini, Y. 1997. Exsolution of magmatic volatile phases from Cl-enriched mineralizing granitic magmas and implications for ore metal transport. *J. Light Metals*, 701-707.

[4] Weckman, D. C. and Niessen, P. 1982. A Numerical Simulation of the DC Continuous Casting Including Nucleate Boiling Heat Transfer. *J. Metal Mater Tran.*, 13B.: 593-602.

[5] Dag Mortensen. 1999. A Mathematical Model of the Heat and Fluid Flows in Direct-Chill Casting of Aluminum Sheet Ingots and Billets. *J. Metal Mater Tran.*, 30B.: 119-133.

[6] Drezet, J. M., Burghardt, A., Fjaer, H. G. and Mabnin, B. 2000. Thermomechanical Effects in DC Casting of Aluminium Alloy: a Numerical Benchmark Study. Materials Science Forum, 329-330: 493.

[7] Drezet, J. M., Rappaz M. and Huglen R. 1997. Direct Chill Casting of Aluminum Alloys : Ingot Distorsion and Mold Design Optimization. *J. Light Metals*, 491.

[8] Prasso, D. C., Evans, J. W. and Wilson, I. 1995. Heat transport and solidification in the electromagnetic casting of aluminum alloys: Part II. Development of a mathematical model and comparison with experimental results. *J. Metal Mater Trans.*, 26B: 1281

[9] Xie, C. L. 2005. "*Theoretical and Experimental Study of the Multi-Strand Low-Frequency Electromagnetic Casting of Aluminum Alloy*". Master Dissertation, Inner Mongolia University of Science and Technology, China.

[10] Dua, Q., Eskina, D. G., and Katgermanb, L. 2005. The Effect of Ramping Casting Speed and Casting Temperature on Temperature Distribution and Melt Flow Patterns in the Sump of DC Cast Billet. *Material Science and Engineering*, 413-414: 144-150.

[11] Lalpoor, M., ESkin, D. G., Ruvalcaba, D., Fjar, H. G., Ten Cate, A., Ontijt, N., and Katgerman, L. 2011. Cold Cracking in DC-Cast High Strength Aluminum Alloy Ingot: An Intrinsic Problem Intensified by Casting Process Parameters. *Material Science and Engineering*, 528-6: 2831-2842.

[12] Adrian Sabau, Kazumori Kuwana Sabau, A., K., Viswanathan, S., Saito, K., and Daris, L. 2004. Heat Transfer Boundary Conditions for the Numerical Simulation of the DC Casting Process in Proceedings of Light Metals. *J. Light Metals*,667-672.